Korean J. Chem. Eng., 33(4), 1391-1401 (2016)
DOI: 10.1007/s11814-015-0232-6

pISSN: 0256-1115
eISSN: 1975-7220

Comparative study of zeolite 5A and zeolite 13X in air separation by pressure swing adsorption

Ehsan Javadi Shokroo*,†, Danial Jafari Farsani, Hadiseh Khalilpour Meymandi*, and Nadia Yadollahi***

*PART-SHIMI Knowledge Based Company, Shiraz, Iran
**Bidboland Refining Co., NIGC, Bidboland, Iran
(*Received 23 June 2015 • accepted 6 November 2015*)

Abstract−The performance of zeolites 5A and 13X is numerically investigated in oxygen separation from air by a two-bed PSA system. The effect of operating variables such as adsorption step time, P_H/P_L ratio and cycle time was investigated on product purity and recovery. The simulation results showed that nitrogen adsorption capacity on zeolite 13X was slightly more than the one on zeolite 5A. In the completely same operating conditions, zeolite 5A had a larger mass transfer zone than zeolite 13X. Therefore, the adsorption and desorption rate of nitrogen on zeolite 5A is less than zeolite 13X. Moreover, for the equal volume of adsorbed nitrogen on both adsorbents, zeolite 5A is more capable rather than zeolite 13X to desorb much more volume of nitrogen at certain time. Furthermore, for achieving oxygen with purity of 96%, utilizing zeolite 5A is more economical than zeolite 13X, when $5.5<P_H/P_L<7$ and $75<$cycle time≤ 90.

Keywords: Pressure Swing Adsorption, Zeolite 5A, Zeolite 13X, Separation, Numerical Simulation

INTRODUCTION

Air separation is one of the most important gas separation processes in the chemical industry. The two most commonly methods used for the separation of oxygen and nitrogen from air are as follows: 1. Cryogenic distillation (by use of the relative volatility difference between two components). 2. Adsorption processes such as pressure swing adsorption (PSA), which works based on the selective adsorption capability of a component on a suitable adsorbent. PSA technology is used to separate some gas species from a gas mixture under pressure according to the molecular characteristics of the species and affinity for an adsorbent material. This process operates at near-ambient temperatures. Specific adsorptive materials such as zeolites, activated carbon, molecular sieves are used as adsorbents to adsorb the target gas species at high pressure. The process then swings to low pressure for the purpose of desorbing the adsorbed material [1].

In addition to PSA, there is also temperature swing adsorption (TSA), which is based on adsorption at operating conditions and regeneration at an elevated temperature. Similar to other adsorption processes, there are at least two stages in TSA processes: adsorption and desorption. Desorption in the cycle of this process includes two stages of heating and cooling. After ending the heating stage, the bed cooling operation starts in order that the first adsorption condition is obtained [1,2].

Generally, the common adsorption processes of air separation are divided into two categories. The first category consists of processes which make use of zeolites as nitrogen adsorbent under the equilibrium conditions and oxygen is a process product. The second one contains processes which utilize carbon molecular sieves (CMSs) as oxygen adsorbent. Based on kinetic separation in this kind of category, oxygen is adsorbed owing to its faster permeation and higher selectivity. Moreover, nitrogen is produced as a product in such these processes. The operating conditions, product purity and type of cycles are completely different in these two categories. As a matter of fact, producing oxygen from air depends on its applications in different industries.

Oxygen is one of the most important products in the chemical industry. This chemical element is used in various processes, such as refineries, manufacturing metal and other industrial operations. For instance, oxygen with high purity is used in different chemical processes like steel construction, paper industries, wastewater treatment and glass production. In 1907, oxygen was produced for the first time, when Linde built a first cryogenic distillation bed for air separation [3].

A widely used unit operation for gas separation or purification is pressure swing adsorption used in most of the commercial adsorption applications [4-8]. Before 1980, PSA systems were used with adsorption pressure greater than atmospheric pressure and desorption pressure near atmospheric conditions. In comparison with cryogenic distillation process, these systems are low-cost in terms of initial investment (because of their simplicity), whereas they are costly in terms of energy consumption. Vacuum swing adsorption (VSA) systems (a kind of operations which work with adsorption pressure of slightly more than atmospheric pressure and desorption pressure of about 0.2 atm) have been developed due to availability of modified adsorbents and the less cost of vacuum equipment, rather than feed compression.

Over the past 40 years, several processes of PSA and VSA systems have been designed in order that pure oxygen from air mix-

†To whom correspondence should be addressed.
E-mail: ehsan.javadi@hotmail.com
Copyright by The Korean Institute of Chemical Engineers.

ture is produced. In O_2-PSA industrial units the ratio of high pressure, in the adsorption step, to low pressure, in the desorption step, (P_H/P_L), is considered to be one of the most important factors owing to determine required energy [9]. Typically, the pressure ratio of 4 and higher than 4 is utilized in the industries. Furthermore, many units with low capacity make use of two-bed systems based on Skarstrom cycle, which are sometimes associated with an equalization step in order to improve the recovery.

Selecting a suitable adsorbent is a critical parameter to design a PSA process. Generally, finding a suitable adsorbent is the first step in developing adsorption separation process. As the separation factor usually varies with temperature and considerably with composition, choosing appropriate conditions for maximizing the separation factor is considered to be a major issue in the process design. Sometimes an initial selection of suitable adsorbents can be directly achieved according to available Henry's law constants.

Most of the time, selecting the adsorbents can be easily achieved with measurement of chromatographic retention times (MCRT). Moreover, to achieve a quick and actual estimation of separation factors, chromatographic methods are better than the other methods because of their prediction in adsorption kinetic.

Zeolites 5A and 13X are the most commonly used adsorbents in air separation for oxygen production. The unique properties of zeolites are originated from this fact that their surfaces are formed with negatively charged oxides. Moreover, the presence of isolated cations above their surface structure is another reason for their uniqueness. Despite knowing the selectivity of O_2/N_2 by zeolite, there was no progress in the case of air separation by adsorption process until 1960 [9], even after the innovation of synthetic zeolites 5A and 13X and PSA cycles. The innovation of zeolites 5A and 13X by Milton (1959) created conditions which were always available [3]. Zeolites are aluminosilicate crystallines of alkaline or earth alkaline elements such as sodium, potassium and calcium. More detailed description of the zeolite structures is accessible in the literature [11]. There are many studies which have been done on the separation of oxygen from air [12-26]. By these innovations, the industrial ideologists were e ncouraged to examine the feasibility of air separation at ambient temperature by applying adsorption processes, while the temperature for cryogenic processes was 77 K. From an economical point of view, the history of PSA technology development can be associated with reducing the cost of oxygen production via this process which is illustrated in Fig. 1.

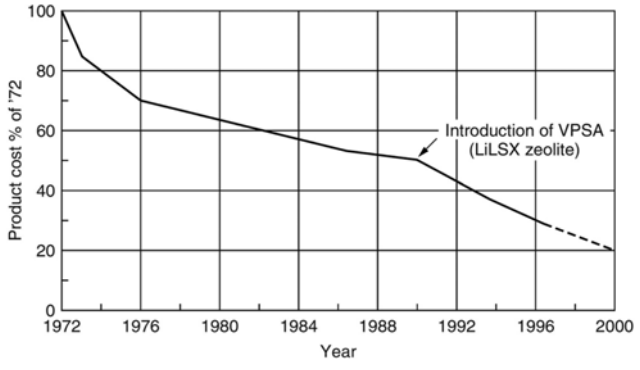

Fig. 1. Cost of oxygen production by applying PSA process (in constant dollars). Zeolites 5A and 13X were used before 1990 and zeolite LiLSX was used afterwards [10].

Several investigations and experimental researches have been separately done in order to separate oxygen from air by PSA process using zeolites 5A and 13X [9]. However, there are not any investigations in accordance with the range of operating conditions of these two adsorbents in order to compare their effects on the process performance. Despite there being many investigations which were performed on the dynamics of a zeolite adsorption and desorption, there are not any investigations on the PSA process performance according to the type of adsorbent. For instance, the adsorption and desorption experiments for N_2/O_2 system on zeolite 5A, 10X, and 13X beds were performed by Jee et al. [27] to study the dynamic characteristics of air separation adsorption processes. Although zeolites 5A and 13X are both commonly used for oxygen separation from air in the PSA process, there are still unanswered questions. For example, whether to use 5A or 13X at different operating conditions when the product purity is more important than recovery. Is zeolite 5A better than zeolite 13X when a product recovery with an acceptable level of purity is considered? Or which type of zeolite should be used when both purity and recovery of oxygen are expected to be in the acceptable range? Answering these important questions requires strong and effective studies which have been investigated in the current study.

Two processes of oxygen separation from air by means of PSA technique, using zeolites 5A and 13X as adsorbents, are simulated at the same operating conditions in this study. The influence of adsorbent type on O_2-PSA process performance is examined. Furthermore, the importance of zeolite type in the quality and quantity of oxygen has been interpreted according to different operational variables. The simulated PSA process is a six-step process with the following sequence: (I) co-current feed pressurization (PR); (II) high-pressure adsorption (AD) step; (III) counter-current depressurizing pressure equalization (ED) step; (IV) counter-current blow down (BD) step; (V) counter-current purge with a light product (PG) step; (VI) co-current pressurizing pressure equalization (EP) step.

MATHEMATICAL MODEL

To develop a mathematical model for a PSA system, the following assumptions were made:

1. Gas behaves as an ideal gas;
2. Total pressure versus time remains constant during adsorption and purge steps;
3. Total pressure changes nonlinearly with time during pressurization, pressure equalization and blow down steps;
4. The flow pattern is axially assumed as plug-flow model;
5. Equilibrium equations for air are expressed as triple Langmuir-Freundlich isotherm (oxygen, nitrogen and argon);
6. Rate of mass transfer is presented by linear driving force (LDF) relations;
7. Bed is clean at initial state and there is no gas flow in it;
8. Air is considered a mixture of oxygen and argon (21%) and nitrogen (79%) as feed.

According to these assumptions, dynamic behavior of system in terms of mass, energy and momentum balances can be expressed

as follows:

Dimensionless partial mass balance for gas phase in the adsorption bed is [9,20,25,26]:

$$-\left(\frac{1}{P_e^m}\right)\cdot\frac{\partial^2 y_i}{\partial \hat{z}^2}+y_i\cdot\frac{\partial \hat{u}}{\partial \hat{z}}+\hat{u}\cdot\left(\frac{\partial y_i}{\partial \hat{z}}+y_i\cdot\left(\frac{1}{\hat{P}}\cdot\frac{\partial \hat{P}}{\partial \hat{z}}-\frac{1}{\hat{T}}\cdot\frac{\partial \hat{T}}{\partial \hat{z}}\right)\right)$$
$$+\frac{\partial y_i}{\partial \tau}+y_i\cdot\left(\frac{1}{\hat{P}}\cdot\frac{\partial \hat{P}}{\partial \tau}-\frac{1}{\hat{T}}\cdot\frac{\partial \hat{T}}{\partial \tau}\right) \quad (1)$$
$$+\left(\frac{\rho_p\cdot R\cdot T_0\cdot\hat{T}}{P_0\cdot\hat{P}}\right)\cdot\left(\frac{1-\varepsilon}{\varepsilon}\right)\cdot\left(q_{m,i}\cdot\frac{\partial \hat{q}_i}{\partial \tau}+\hat{q}_i\cdot\frac{\partial q_{m,i}}{\partial \tau}\right)=0$$

Dimensionless equilibrium loading of i^{th} component for solid phase in the adsorption bed is:

$$\frac{\partial q_{m,i}}{\partial \tau}=\frac{\partial q_{m,i}}{\partial \hat{T}}\times\frac{\partial \hat{T}}{\partial \tau}=k_{2,i}T_0\times\frac{\partial \hat{T}}{\partial \tau} \quad (2)$$

Dimensionless loading of i^{th} component for solid phase in the adsorption bed is (LDF relation):

$$\frac{\partial \hat{q}_i}{\partial \tau}=\alpha_i\cdot\left(\frac{\beta_i\cdot y_i^{ni}}{1+\sum_{j=1}^{N}\beta_j\cdot y_j^{nj}}-\hat{q}_i\right)-\left(\frac{\hat{q}_i}{q_{m,i}}\cdot\frac{\partial q_{m,i}}{\partial \tau}\right) \quad (3)$$

According to Eq. (3), the LDF relation depends on various parameters, such as equilibrium parameter for the Langmuir model, mole fraction of species i in the gas phase, average amount adsorbed and equilibrium parameter for the Langmuir model.

The equilibrium of triple Langmuir-Freundlich isotherm is as follows:

$$\hat{q}_i^*=\frac{\beta_i y_i^{ni}}{1+\sum_{j=1}^{N}\beta_j\cdot y_j^{nj}} \quad (4)$$

where β, n and q_m are as follows:

$$q_{m,i}=k_1+k_2T_0\hat{T} \quad (5)$$

$$\beta_i=k_3\exp\left(\frac{k_4}{T_0\hat{T}}\right) \quad (6)$$

$$n=k_5+\frac{k_6}{T_0\hat{T}} \quad (7)$$

Table 1. Equilibrium parameters and adsorption heat of oxygen, nitrogen and argon on zeolites 5A and 13X

Parameters	Zeolite 5A [21,22]		Zeolite 13X [20]	
	N_2	O_2	N_2	O_2
$k_1\times10^3$ (mol/g)	6.21	7.252	12.52	6.705
$k_2\times10^5$ (mol/g·K)	−1.27	−1.820	−1.785	−1.435
$k_3\times10^4$ (1/atm)	1.986	54.19	2.154	3.253
k_4 (K)	1970	662.6	2333	1428
k_5	2.266	−1.101	1.666	−0.3169
k_6 (K)	−396.5	656.4	−245.2	387.8
Heat of adsorption (cal/mol)	5470	3160	4390	3060
LDF constant (s^{-1})	0.05	0.15	0.197	0.62

Adsorption isotherm parameters and diffusion rate constants of oxygen, nitrogen and argon over zeolites 5A and 13X are presented in Table 1.

Overall dimensionless mass balance for gas phase in the adsorption bed is [12,19,23,28]:

$$\left(\frac{1}{\hat{P}}\right)\cdot\frac{\partial \hat{P}}{\partial \tau}+\frac{\partial \hat{u}}{\partial \hat{z}}+\frac{\hat{u}}{\hat{P}}\cdot\frac{\partial \hat{P}}{\partial \hat{z}}-\left(\frac{1}{\hat{T}}\right)\cdot\left(\frac{\partial \hat{T}}{\partial \tau}+\hat{u}\frac{\partial \hat{T}}{\partial \hat{z}}\right)$$
$$+\left(\frac{\rho_p\cdot R\cdot T_0\cdot\hat{T}}{P_0\cdot\hat{P}}\right)\cdot\left(\frac{1-\varepsilon}{\varepsilon}\right)\cdot\sum_{i=1}^{3}\left(q_{m,i}\cdot\frac{\partial \hat{q}_i}{\partial \tau}+\hat{q}_i\cdot\frac{\partial q_{m,i}}{\partial \tau}\right)=0 \quad (8)$$

Dimensionless energy balance for gas phase in the adsorption bed is [13-15,18,24]:

$$-\left(\frac{1}{P_e^h}\right)\cdot\frac{\partial^2 \hat{T}}{\partial \hat{z}^2}+\varepsilon\cdot\left(\hat{u}\frac{\partial T}{\partial z}+\hat{T}\frac{\partial \hat{u}}{\partial \hat{z}}\right)+\left(\varepsilon_t+\frac{\rho_B\cdot c_{p,s}}{\rho_g\cdot c_{p,g}}\right)\cdot\frac{\partial \hat{T}}{\partial \tau}$$
$$-\left(\frac{\rho_B}{T_0\cdot\rho_g\cdot c_{p,g}}\right)\cdot\sum_{i=1}^{3}\left[\left(q_{m,i}\cdot\frac{\partial \hat{q}_i}{\partial \tau}+\hat{q}_i\cdot\frac{\partial q_{m,i}}{\partial \tau}\right)\cdot(-\Delta\overline{H}_i)\right] \quad (9)$$
$$+\left(\frac{2h_i\cdot L}{R_{B,i}\cdot U_0\cdot\rho_g\cdot c_{p,g}}\right)\cdot(\hat{T}-\hat{T}_w)=0$$

Dimensionless energy balance for the wall of adsorption bed is:

$$\frac{\partial \hat{T}_w}{\partial \tau}=\left[\frac{2\pi\cdot R_{B,i}\cdot h_i\cdot L}{\rho_w\cdot c_{p,w}\cdot A_w\cdot U_0}\right]\cdot(\hat{T}-\hat{T}_w)$$
$$-\left[\frac{2\pi\cdot R_{B,o}\cdot h_o\cdot L}{\rho_w\cdot c_{p,w}\cdot A_w\cdot U_0}\right]\cdot\left(\hat{T}_w-\frac{T_{atm}}{T_0}\right) \quad (10)$$

Cross-sectional area of adsorption bed wall is:

$$A_w=\pi\cdot(R_{B,o}^2-R_{B,i}^2) \quad (11)$$

Dimensionless boundary conditions for mass and energy balances are as follows:

Pressurization and adsorption steps:

$$\left(\frac{\partial y_i}{\partial \hat{z}}\right)\Big|_{\hat{z}=0}=-P_e^m\cdot\hat{u}\cdot(y_i|_{\hat{z}=0^-}-y_i|_{\hat{z}=0^+});\ \frac{\partial y_i}{\partial \hat{z}}\Big|_{\hat{z}=1}=0 \quad (12)$$

$$\left(\frac{\partial \hat{T}}{\partial \hat{z}}\right)\Big|_{\hat{z}=0}=-P_e^h\cdot\hat{u}\cdot(\hat{T}|_{\hat{z}=0^-}-\hat{T}|_{\hat{z}=0^+});\ \frac{\partial \hat{T}}{\partial \hat{z}}\Big|_{\hat{z}=1}=0 \quad (13)$$

$y_i|_{z=0^-}$ and $T|_{z=0^-}$ are composition of i^{th} component in the inlet feed and the feed temperature in Eqs. (12) and (13), respectively.

Blow down and equalization to depressurization steps:

$$\frac{\partial y_i}{\partial \hat{z}}\Big|_{\hat{z}=0}=\frac{\partial y_i}{\partial \hat{z}}\Big|_{\hat{z}=1}=0;\ \frac{\partial \hat{T}}{\partial \hat{z}}\Big|_{\hat{z}=0}=\frac{\partial \hat{T}}{\partial \hat{z}}\Big|_{\hat{z}=1}=0 \quad (14)$$

Purge step:

$$\left(\frac{\partial y_i}{\partial \hat{z}}\right)\Big|_{\hat{z}=0}=0;\ \left(\frac{\partial y_i}{\partial \hat{z}}\right)\Big|_{\hat{z}=1}=-P_e^m\cdot\hat{u}\cdot(y_i|_{\hat{z}=1^+}-y_i|_{\hat{z}=1^-}) \quad (15)$$

$$\left(\frac{\partial \hat{T}}{\partial \hat{z}}\right)\Big|_{\hat{z}=0}=0;\ \left(\frac{\partial \hat{T}}{\partial \hat{z}}\right)\Big|_{\hat{z}=1}=-P_e^h\cdot\hat{u}\cdot(\hat{T}|_{\hat{z}=1^+}-\hat{T}|_{\hat{z}=1^-}) \quad (16)$$

where, $y_i|_{z=L^+}$ and $T|_{z=L^+}$ are concentration of the i^{th} component in the product of AD step and the output flow temperature of AD step, respectively.

Equalization to pressurization step:

$$\left(\frac{\partial y_i}{\partial \hat{z}}\right)\Big|_{\hat{z}=0} = -P_e^m \cdot \hat{u} \cdot (y_i|_{\hat{z}=0^-} - y_i|_{\hat{z}=0^+}); \frac{\partial y_i}{\partial \hat{z}}\Big|_{\hat{z}=1} = 0 \quad (17)$$

$$\left(\frac{\partial \hat{T}}{\partial \hat{z}}\right)\Big|_{\hat{z}=0} = -P_e^h \cdot \hat{u} \cdot (\hat{T}|_{\hat{z}=0^-} - \hat{T}|_{\hat{z}=0^+}); \frac{\partial \hat{T}}{\partial \hat{z}}\Big|_{\hat{z}=1} = 0 \quad (18)$$

$y_i|_{z=0^-}$ and $T|_{z=0^-}$ are concentration of i^{th} component in the outlet flow of ED step and the outlet flow temperature of ED step in Eqs. (17) and (18), respectively.

Ergun equation is utilized to investigate the pressure drop across the adsorption bed [16,17].

$$-\frac{d\hat{P}}{d\hat{z}} = [a \cdot \mu \cdot U_0 \cdot \hat{u} + b \cdot \rho \cdot U_0^2 \cdot \hat{u} \cdot |\hat{u}|] \cdot \left(\frac{L}{P_0}\right) \quad (19)$$

$$a = \frac{150}{4R_p^2} \cdot \frac{(1-\varepsilon)^2}{\varepsilon^2}; \; b = 1.75\frac{(1-\varepsilon)}{2R_p\varepsilon} \quad (20)$$

Moreover, a non-linear equation for variable pressure step is used to study the pressure changes versus dimensionless time [16,17]:

$$\hat{P}(\tau) = A \cdot \tau^2 + B \cdot \tau + C \quad (21)$$

Physical properties of adsorbents and characteristics of adsorption bed are depicted in Tables 2 and 3, respectively.

RESULTS AND DISCUSSION

The fourth-order Runge-Kutta Gill scheme was used to solve a mathematical model considered as coupled partial differential equations. The experimental data obtained from the literature has been simulated to validate the simulation results in this study [17,20,21]. An experimental and simulation study of a PSA unit which is running a traditional Skarstrom cycle and a Skarstrom cycle with co-current equalization owing to separate oxygen from air using a 5A zeolite has been proposed by Mendes et al. in 2001.

Table 2. Physical properties of beds and adsorbents

Characteristic	Zeolite 5A [21,22]	Zeolite 13X [20]
Type	Sphere	Sphere
Average pellet size, R_P (cm)	0.157	0.07
Pellet density, ρ_p (g/cm^3)	1.16	1.17
Heat capacity, C_{ps} (cal/g·K)	0.32	0.32
Bed porosity, ε	0.314	0.391
Bed density, ρ_B (g/cm^3)	0.795	0.713

Table 3. Adsorption bed properties [29]

Length, L (cm)	76
Inside radius, R_{Bi} (cm)	2.138
Outside radius, R_{Bo} (cm)	2.415
Heat capacity of the column, C_{pw} (cal/g·K)	0.12
Density of column, ρ_w (g/cm^3)	7.83
Internal heat-transfer coefficient, h_i (cal/cm^2·K·s)	9.2×10^{-4}
External heat-transfer coefficient, h_o (cal/cm^2·K·s)	3.4×10^{-4}
Axial thermal conductivity, K_L (cal/cm·s·K)	6.2×10^{-5}
Axial dispersion coefficient, D_L (cm^2/s)	1×10^{-5}

The effects of production pressure, purge and product flow rates, and production step duration on the product purity and recovery are investigated for both cycles and compared. Furthermore, a lin-

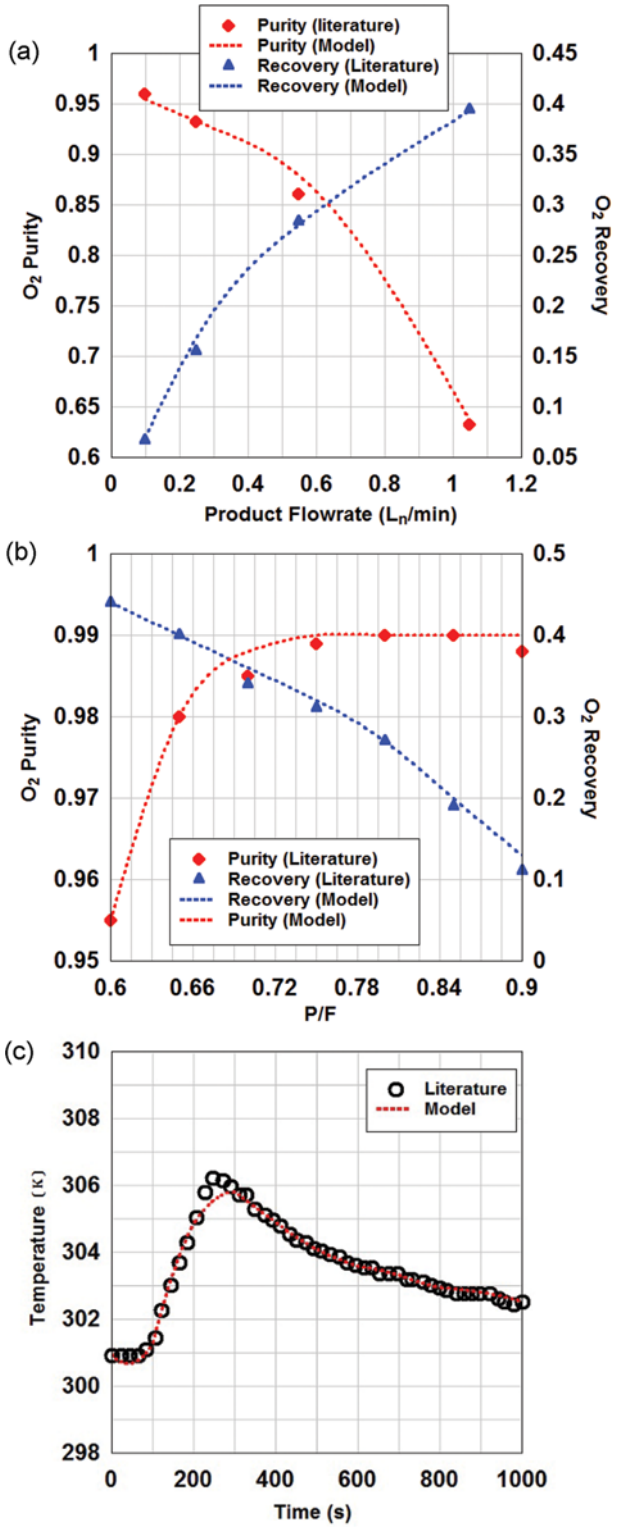

Fig. 2. (a) Numerical simulation of experimental data in this work [17]. (b) Numerical simulation of experimental data in this work [20]. (c) Numerical simulation of experimental data in this work [21].

ear driving force representation of the dusty gas intra particle mass transport is considered in their model [17]. Moreover, a small-scale two-bed six-step PSA process using zeolite 13X was performed by Jee et al. to provide oxygen-enriched air. The effects of different operating parameters such as the P/F ratio, adsorption pressure, feed flow rate, and adsorption step time were investigated experimentally under the nonisothermal condition. They showed that there is a strong effect of feed flow rate on O_2 purity [20]. The effects of adsorption and desorption on zeolite 5A and CMS beds were investigated in a mixture of N_2/O_2/Ar by Jee et al. in 2004. A non-isothermal mathematical model was applied to simulate the adsorption dynamics in their studies [21].

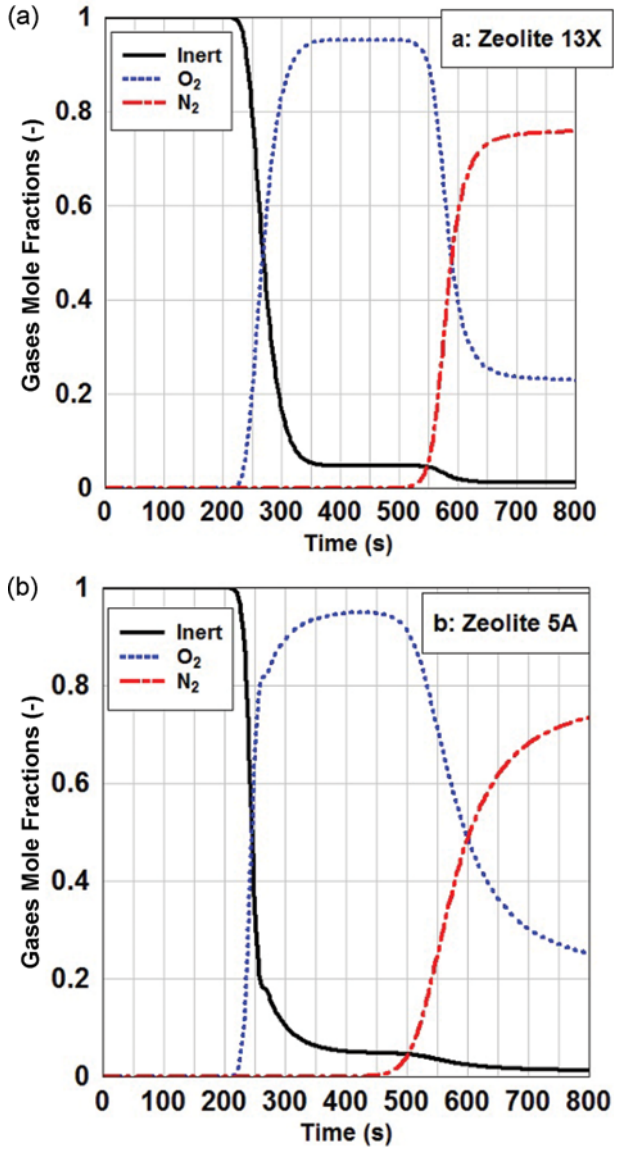

Fig. 3. (a) The simulated breakthrough curves of zeolite 13X for oxygen and nitrogen at adsorption pressure of 6 bar and feed flow rate of 5 LSTP/min. The adsorption bed was initially saturated with a non-adsorptive gas. (b) The simulated breakthrough curves of zeolite 5A for oxygen and nitrogen at adsorption pressure of 6 bar and feed flow rate of 5 LSTP/min. The adsorption bed was initially saturated with a non-adsorptive gas.

Figs. 2(a) and (b) indicate the effect of product flow rate and P/F on the purity and recovery of oxygen during PSA process, respectively. The impact of temperature variations in gas phase during adsorption as a function of time is illustrated in Fig. 2(c). It is obviously seen that there is a relatively high accuracy in the simulation of experimental data [29]. Breakthrough curves for nitrogen and oxygen on both zeolites 13X and 5A are shown in Figs. 3(a) and (b), respectively. The term "break-through time" is originated from the response of initially cleaned bed per a flow with a constant composition. As an initial condition, it is assumed that the adsorption bed is pressurized with a non-adsorptive gas. As shown in Fig. 3(a), oxygen exits from the top of zeolite 13X earlier than nitrogen at a time of approximately 230 seconds [29].

As time is passing, high roll-up phenomenon is observed in the case of oxygen. Owing to high roll-up phenomenon effect, oxygen concentration is approximately 4.5 times more than feed concentration during the time of 400-500 seconds. Occurring high roll-up phenomenon in the case of oxygen is because there is a competitive adsorption between oxygen and nitrogen molecules to be adsorbed on the adsorbent.

This competitive adsorption can be developed according to nitrogen and oxygen properties like polarizability, dipole moment and quadruple moment. The isotropic polarizability is defined as the average of the diagonal terms of the polarizability tensor. Nitrogen and oxygen molecules are symmetrical and thus they are not dipole. Both of these molecules are diatomic molecules. The polarizability of oxygen and nitrogen is 1.562 and 1.710 ($Å^3$), respectively. Furthermore, the bond description of oxygen molecule is double bond (O=O); however, the nitrogen bond description is triple bond (N#N). Moreover, the electric quadruple moment of nitrogen is (xx, yy, zz)=(0.697, 0.697, −1.394). Besides, the molecular diameters of oxygen and nitrogen are 3.8 Å and 4.2 Å, correspondingly [30].

The adsorption kinetics and equilibrium have been investigated in this study. In fact, the adsorption capacity will be greater for more polarity molecules which is consistent with adsorption equilibrium. On the other hand, the rate of adsorption will be greater for molecules with smaller sizes, which is based on the adsorption kinetics.

The superiority of adsorption equilibrium mechanism than adsorption kinetic mechanism in zeolite adsorbents for separation of oxygen and nitrogen has been depicted in the literature [1].

Oxygen is affected by the high roll-up phenomenon because nitrogen adsorption on the adsorbent sites is much more than oxygen adsorption. Therefore, oxygen concentration is relatively increased rather than feed concentration. While time reaches nitrogen breakthrough at the time of 550 seconds, oxygen concentration is starting to be reduced. As clearly shown in Fig. 3(a), the high roll-up phenomenon does not occur in the case of nitrogen due to its strong adsorption on zeolite 13X adsorbent. Fig. 3(b) presents the breakthrough curves in zeolite 5A. According to this figure, although oxygen penetration on zeolite 5A is similar to the one on zeolite 13X, nitrogen penetration occurs at the time of 450 seconds. By comparing Figs. 3(a) and 3(b), the breakthrough curves for zeolite 5A is slightly broader than zeolite 13X. In addition, the

capacity of nitrogen adsorption on zeolite 13X is slightly more than the one on zeolite 5A. Moreover, the high roll-up phenomenon occurs in both zeolites 5A and 13X in the case of oxygen. The adsorption capacity in the adsorption bed depends on the factors such as pressure, temperature, flow rate [9,20]. Actually, the adsorption and desorption cycle of a PSA system operates by pressure increasing and decreasing. Adsorption and desorption phenomenon are inherently exothermic and endothermic, respectively. Therefore, the optimal setting of temperature is very important owing to better performance of adsorption and desorption phenomenon. On the other hand, the adsorption of impurities on the adsorbent bed is a function of retention time on the adsorbent. Consequently, the flow rate factor is necessary for better performance of system.

The concentration of nitrogen on zeolites 13X and 5A in terms of different adsorption pressures and time are presented in Figs. 4(a) and (b), respectively. As pressure increases, the adsorption rate of more strongly adsorbed component increases [9,20]. As it is expected, nitrogen adsorption capacity on zeolites 13X and 5A enhances with pressure increasing. Although nitrogen adsorption capacity is approximately the same on both adsorbents, nitrogen breakthrough on zeolite 13X occurs with a steeper slope rather than zeolite 5A in different adsorption pressures. Furthermore, the effect of increasing the adsorption pressure on zeolite 13X is more effective than the other zeolite and the adsorption capacity increases gradually. Therefore, the rate of nitrogen adsorption on zeolite 13X is more than the one on zeolite 5A due to different kinetic parameters of these two zeolites. It is depicted in Table 1 that the nitrogen LDF coefficient for zeolite 13X is almost four-times more than the one on zeolite 5A. On the other hand, the rate of nitrogen adsorption on zeolite 13X is approximately four-times more than the one on zeolite 5A in the completely same conditions. The difference in the rate of adsorption can be investigated in the different mass transfer zones (MTZs) of these two zeolite beds.

Oxygen concentration along the bed length for zeolites 13X and 5A in different times have been depicted in Figs. 5(a) and (b), respectively. Obviously, the slope of oxygen concentration curves in the case of zeolite 13X is faster than zeolite 5A. On the other hand, there is a larger MTZ for zeolite 5A rather than zeolite 13X in the

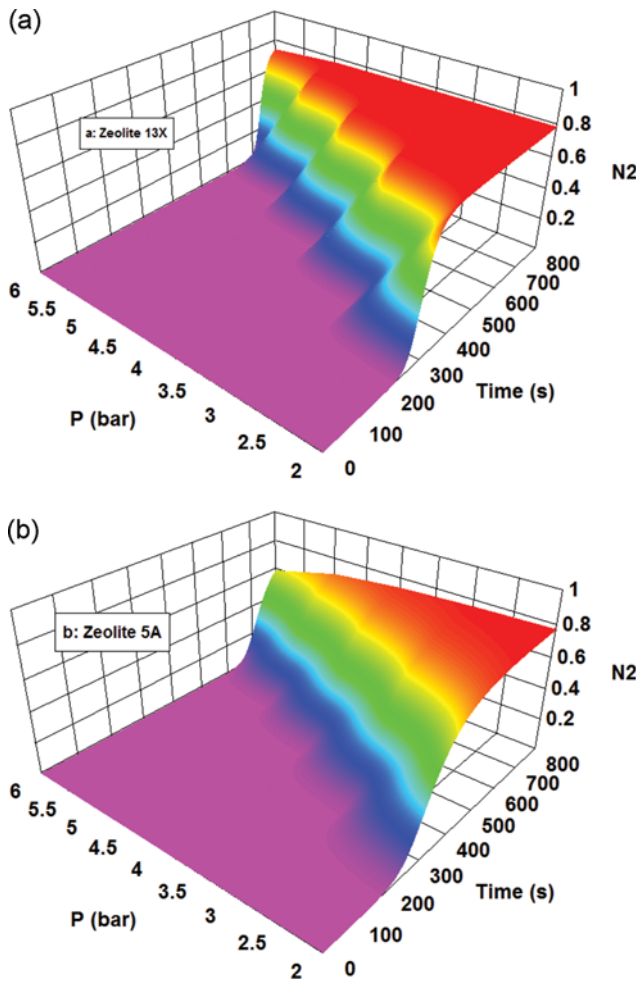

Fig. 4. (a) The outlet mole fraction of nitrogen form zeolite 13X at different adsorption pressures and feed flow rate of 4 LSTP/min. The adsorption bed was initially saturated with a non-adsorptive gas. (b) The outlet mole fraction of nitrogen form zeolite 5A at different adsorption pressures and feed flow rate of 4 LSTP/min. The adsorption bed was initially saturated with a non-adsorptive gas.

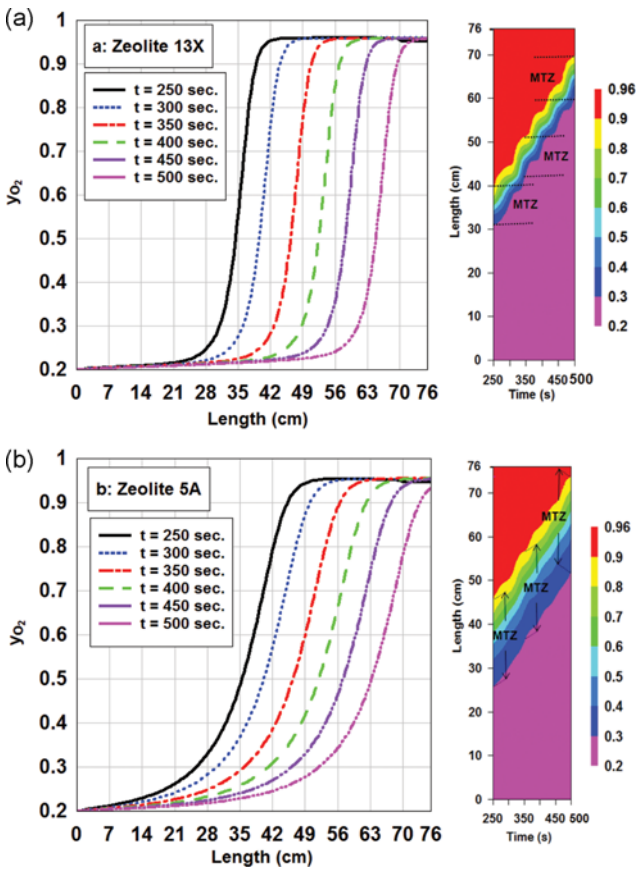

Fig. 5. (a) Distribution of oxygen concentration along the length of zeolite 13X during adsorption process in different times. The feed flow rate is 5 LSTP/min and the adsorption pressure is 6 bar. (b) Distribution of oxygen concentration along the length of zeolite 5A during adsorption process in different times. The feed flow rate is 5 LSTP/min and the adsorption pressure is 6 bar.

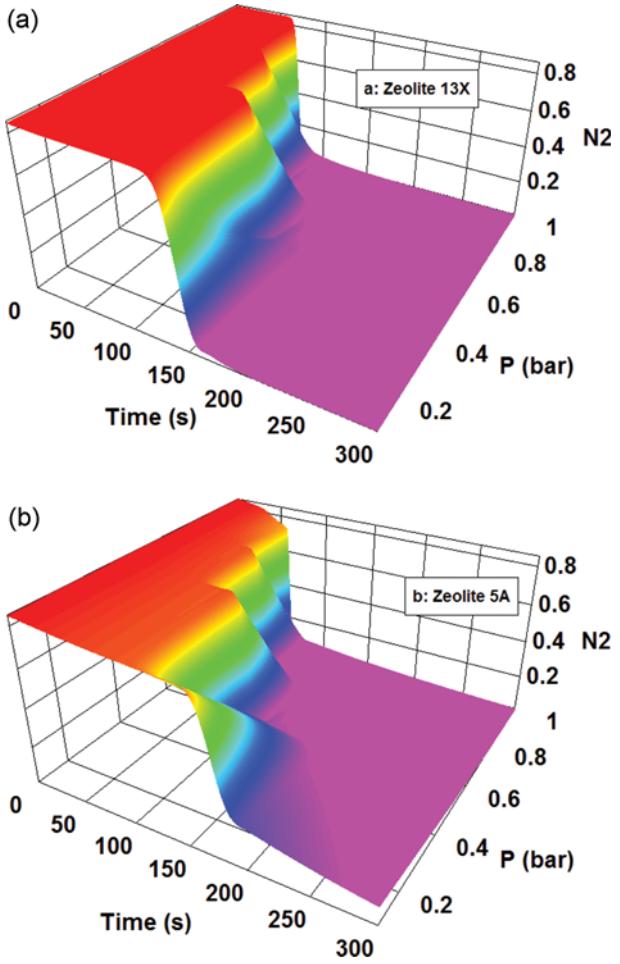

Fig. 6. (a) The outlet simulated concentration of gas phase from zeolite 13X during desorption at pressure of 0.1 bar. The desorption bed was completely clean in the initial state. (b) The outlet simulated concentration of gas phase from zeolite 5A during desorption at pressure of 0.1 bar. The desorption bed was completely clean in the initial state.

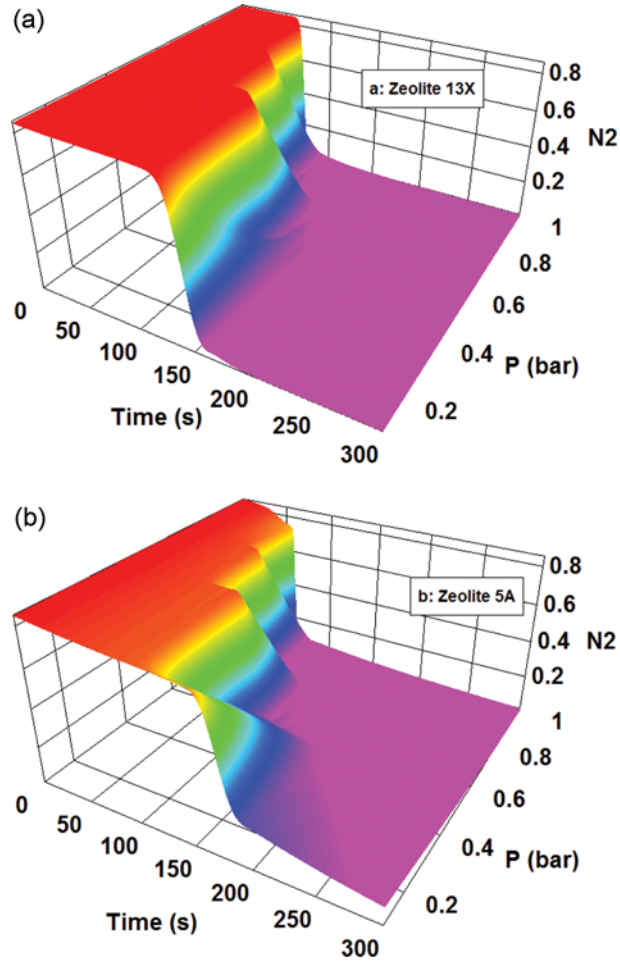

Fig. 7. (a) The outlet concentration of nitrogen from zeolite 13X in the gas phase as a function of desorption pressure and time. Desorption process is applied with a non-adsorptive gas. (b) The outlet concentration of nitrogen from zeolite 5A in the gas phase as a function of desorption pressure and time. Desorption process is applied with a non-adsorptive gas.

completely equal conditions. The bed with smaller MTZ has larger adsorption rate in the completely same conditions [9,20,22]. Moreover, it is considerable to mention that the transfer rate of MTZ is almost equal for both adsorbents.

In the dynamic study of adsorption beds it is considerable to investigate desorption curves. The desorption curves of zeolites 13X and 5A are illustrated in Figs. 6(a) and (b), respectively. To simulate desorption over the beds, it is assumed that a pure inert gas is utilized for cleaning the beds. By passing the inert gas through the bed in a pressure of 0.1 bar, nitrogen with high concentration is first desorbed from top of the bed. As nitrogen is desorbed, a little adsorbed oxygen is removed from the bed with nitrogen. As time passes and the desorbed volume of nitrogen and oxygen gases decreases, the concentration of inert gas in the outlet of bed begins to increase. By comparing Figs. 6(a) and (b), it is considerable to point out:

1. The main drop of nitrogen concentration in the outlet of zeolite 13X occurs at the time of about 125 seconds, while this concentration drop in the outlet of zeolite 5A occurs at the time of about 155 seconds;

2. However nitrogen concentration in the outlet of zeolite 13X approaches zero after about 180 seconds, nitrogen concentration in the outlet of zeolite 5A does not approach zero after approximately 300 seconds and its value is almost 10%.

Besides, according to these figures, nitrogen desorption capacity from zeolite 5A is more than zeolite 13X. On one hand, for the equal volume of adsorbed nitrogen on adsorbents, zeolite 5A is more capable than zeolite 13X owing to desorb much more volume of nitrogen in a certain time. This can be justified in the adsorption and desorption hysteresis loops of zeolites 13X and 5A. On the other hand, in the completely same conditions, the rate of nitrogen desorption from zeolite 13X is more than the one on zeolite 5A owing to smaller MTZ in zeolite 13X rather than zeolite 5A. Similarly to adsorption capacity, the desorption capacity in adsorbent beds depends on some parameters such as pressure, temperature, time, flow rate [9,20], which have been described in details

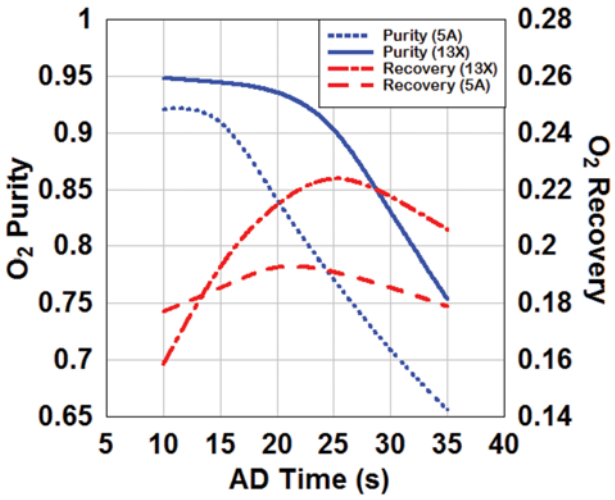

Fig. 8. The simulated purity and recovery of oxygen as a function of adsorption time. The feed flow rate is 20 LSTP/min, adsorption pressure is 6 bar, desorption pressure is 1 bar and the ratio of P/F is 0.1. ED and BD time steps are 5 and 15 seconds, respectively.

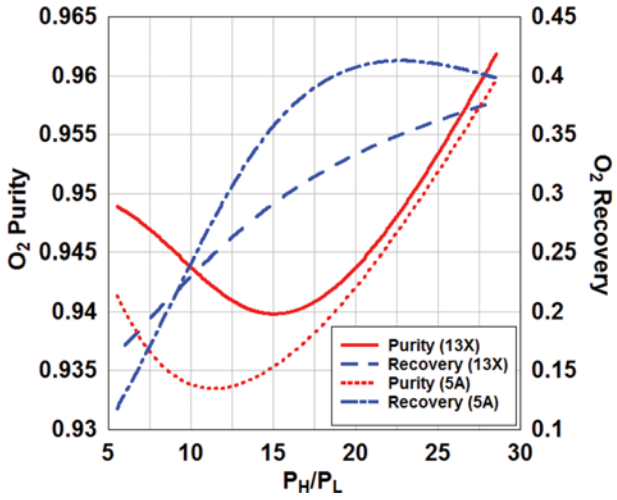

Fig. 9. The simulated purity and recovery of oxygen versus the ratio of operational pressures. The feed flow rate is 2 LSTP/min and the ratio of P/F is 0.1. ED and BD time steps are 5 and 15 seconds, respectively.

above.

Figs. 7(a) and (b) propose nitrogen concentration in the bed outlets for different desorption pressures as a function of time. The desorption amount of more strongly adsorbed component reduces by increasing the pressure [9,20]. As expected, nitrogen desorption capacity from both zeolites 13X and 5A increases by reducing the pressure. Despite the rate of nitrogen desorption from zeolite 13X is more than zeolite 5A, the capacity of nitrogen desorption from zeolite 5A is more than the one on zeolite 13X. As mentioned above, the adsorption capacity and the rate of adsorption are based on molecules with more polarity and molecules with small sizes, respectively. Therefore, there is smaller pore size on zeolite 13X rather than zeolite 5A. In addition the polarity of zeolite 5A is more than zeolite 13X [11]. The importance of this issue can be followed in product recovery and productivity curves.

Fig. 8 shows oxygen purity and recovery as a function of adsorption time for both zeolites. As obvious, there is a light effect on oxygen purity for both adsorbents with increasing the adsorption time at first. Afterwards, the product purity begins to decline with a sharp slope by increasing the time more than 15 and 20 seconds for zeolites 5A and 13X, respectively. The reason for oxygen purity behavior versus the adsorption time is due to breakthrough time. In the PSA process, the adsorption time is determined according to the study on breakthrough curves. In fact, the adsorption time is a required time for occurring breakthrough time. After this time, the product purity decreases while the entire capacity of the bed has not been utilized before this time.

Therefore, the adsorption time must be close to the breakthrough time in order that the best process performance in terms of adsorption time is achieved [31]. The rate of oxygen recovery for both adsorbents increases at first and then it reduces. It is considerable to note that the slope of recovery curve for zeolite 13X is gradually greater than zeolite 5A in incremental zone, while the slope of recovery curve is approximately equal for both zeolites in decreased zone. It is depicted that the performance of a PSA system for oxygen separation from air can work better, where zeolite 13X is utilized under simulated operational conditions. Fig. 9 shows the effect of O_2-PSA system performance versus P_H/P_L for a 60-second cycle. Where $8>P_H/P_L$, the performance of PSA process in terms of oxygen purity and recovery on zeolite 13X is better than zeolite 5A. This result can also validate the curve behavior in Fig. 8. Where $8\leq P_H/P_L\leq 28.5$, the rate of product recovery using zeolite 5A is more than zeolite 13X. Moreover, it is better to apply $25\leq P_H/P_L\leq 28.5$ (VSA system), for both adsorbents, in order to achieve oxygen with high purity and recovery. It occurs because purity and recovery are at their maximum values in Fig. 9. The high value of P_H/P_L ratio for N_2/O_2 system gives the meaning of VSA system. Because pressure higher than 6 bar is not required for oxygen production in a PSA system, which is considered as a zeolite adsorbent system [9]. Due to this fact, when the value of P_H/P_L is high, the desorption pressure is approximately zero which is VSA system. When a VSA system is utilized, the desorption phenomenon is done in vacuum conditions due that the adsorbents are well decontaminated in the desorption step. Therefore, the purity in the adsorption step and recovery will reach their maximum values.

Consequently, the overall results obtained from Fig. 9 are as follows:

1. It is better to apply zeolite 13X in O_2-PSA system to achieve an optimal process performance in terms of product purity and recovery in the range of $5\leq P_H/P_L\leq 8$ in comparison with zeolite 5A.

2. Applying a PSA system in the range of $8\leq P_H/P_L\leq 28.5$ with zeolite 5A operates better than zeolite 13X, when much more oxygen recovery is considered. Note that the performance of mentioned unit will improve by increasing the ratio of P_H/P_L (in Fig. 9, the optimal ratio of P_H/P_L is 22.5).

3. The performance of oxygen separation unit using a VSA system ($25\leq P_H/P_L\leq 28.5$) is almost the same for both zeolites 13X and 5A.

Cycle time is another variable which is effective for the performance of the PSA unit in oxygen separation from air. Figs. 10(a) and (b) show that oxygen purity depends on cycle time in differ-

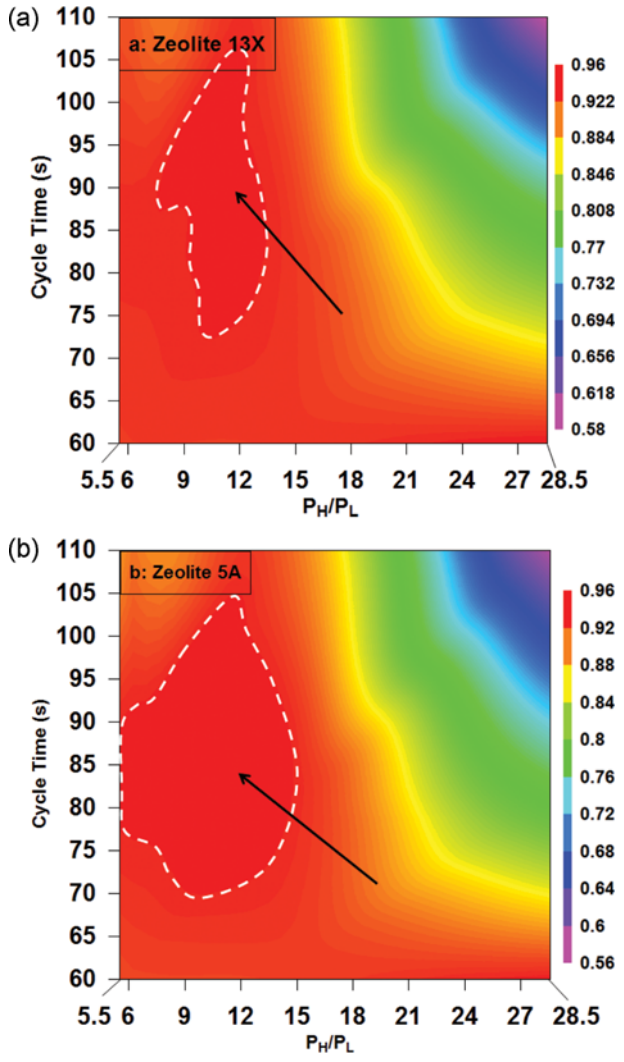

Fig. 10. (a) The distribution of oxygen concentration versus the ratio of operational pressures in different cycle times for zeolite 13X. The product flow rate is 2 LSTP/min and the ratio of P/F is 0.1. (b) The distribution of oxygen concentration versus the ratio of operational pressures in different cycle times for zeolite 5A. The product flow rate is 2 LSTP/min and the ratio of P/F is 0.1.

ent ratios of P_H/P_L for both zeolites 13X and 5A, respectively. The difference in PSA process performance in oxygen separation utilizing zeolites 5A and 13X can be seen by white dashed line in the surrounded area in Figs. 10(a) and (b). Applying higher cycle time and adjusting the ratio of $15>P_H/P_L$ leads to high purity product. According to the definition, the productivity of the PSA unit over the utilized adsorbent is the ratio of received product rate to the used cycle time [20].

On one hand, applying a higher cycle time will increase the unit productivity. On the other hand, increasing the ratio of P_H/P_L will increase the operating costs.

It is suggested that at a low ratio of P_H/P_L and with respect to maintaining high product purity, it is possible to increase the cycle time. According to the white dashed line in the surrounded area in Figs. 10(a) and (b), it is understandable that zeolite 5A is more economical than zeolite 13X when a higher cycle time is applied, because the cycle time can be increased at a low ratio of P_H/P_L. Accordingly, applying zeolite 5A is more economical than zeolite 13X while $5.5<P_H/P_L<7$ and 75<cycle time≤90, in order that oxygen purity of 96% is achieved.

CONCLUSIONS

Two types of zeolites, zeolite 5A and zeolite 13X, were simulated in a laboratory scale of PSA unit in the same operational conditions. Desorption and adsorption dynamics of zeolites 5A and 13X were investigated to study the behavior of these zeolites. Furthermore, the dependency of PSA process performance in terms of product purity and recovery over operational variables such as adsorption time, P_H/P_L and cycle time was compared in this study.

The results obtained from dynamic simulation of beds showed that:

The breakthrough curves for zeolite 5A are broader than zeolite 13X. Moreover, nitrogen adsorption capacity on zeolite 13X is relatively more than the one on zeolite 5A. In addition, the high roll-up phenomenon occurs for both zeolites in the case of oxygen. There is a larger mass transfer zone (MTZ) for zeolite 5A rather than zeolite 13X in the completely same conditions. Therefore, the adsorption rate of zeolite 13X is much more than the one on zeolite 5A. The rate of nitrogen desorption from zeolite 13X is more than zeolite 5A owing to its smaller MTZ. On the other hand, for equal volume of adsorbed nitrogen on the both adsorbents, zeolite 5A is more capable to desorb much more volume of nitrogen rather than zeolite 13X at certain time.

The effect of P_H/P_L on PSA process performance was modeled. The results obtained from this simulation are as follows:

1. Zeolite 13X is more effective than zeolite 5A in the O_2-PSA system. Furthermore, an optimal process performance in terms of product purity and recovery in the range of $5\le P_H/P_L\le 8$ is achieved by applying zeolite 13X rather than zeolite 5A.

2. The performance of zeolite 5A in the range of $8\le P_H/P_L\le 28.5$ in a PSA system is more effective than zeolite 13X. Note that the performance of a PSA system will improve via increasing the ratio of P_H/P_L.

3. It is shown that in a VSA system ($25\le P_H/P_L\le 28.5$), the performance of oxygen separation unit is approximately identical by applying both zeolites 5A and 13X.

Furthermore, simulation results of the cycle time effects showed that:

Applying zeolite 5A is more economical than zeolite 13X in order to achieve oxygen with purity of 0.96, when $5.5<P_H/P_L<7$ and 75<cycle time≤90.

ACKNOWLEDGEMENT

The authors gratefully acknowledge BIDBOLAND refinery plant is in agreement with this research.

NOMENCLATURE

A_w : cross-sectional area of the wall [cm^2]

AD : adsorption step
BD : blow down step
Cp_g, C_{ps}, C_{pw} : gas, pellet, and wall heat capacities, respectively [cal/g·K]
D_L : axial dispersion coefficient [cm^2/s]
G : purge to feed ratio [kg_{feed}/kg_{purge}]
hi : internal heat-transfer coefficient [$cal/cm^2 \cdot K \cdot s$]
ho : external heat-transfer coefficient [$cal/cm^2 \cdot K \cdot s$]
$\Delta\overline{H}$: average heat of adsorption [cal/mol]
k_1 : parameter for the LDF model [mol/g]
k_2 : parameter for the LDF model [mol/g·K]
k_3 : parameter for the LDF model [1/atm]
k_4 : parameter for the LDF model [K]
k_5 : parameter for the LDF model [-]
k_6 : parameter for the LDF model [K]
K_L : axial thermal conductivity [cal/cm·s·K]
L : bed length [cm]
P : total pressure [atm]
$\overline{P}$: dimensionless pressure [P/P_0]
P_e^h : heat peclet number [$u_0 \cdot L \cdot \rho_g \cdot c_{p,g}/K_L$]
P_e^m : mass peclet number [$u_0 \cdot L/D_L$]
P_r : reduced pressure, dimensionless
PG : purge step
PR : pressurization step
P/F : ratio of purge flow rate to feed flow rate
P_H/P_L : ratio of operating pressures
q, q*, $\hat{q}$: amount adsorbed, equilibrium amount adsorbed, and average amount adsorbed, respectively [mol/g]
q_m : equilibrium parameter for the Langmuir model [mol/g]
R : gas constant [cal/mol·K]
R_p : radius of the pellet [cm]
R_{Bi}, R_{Bo} : inside and outside radial of the bed, respectively [cm]
T : temperature [K]
$\overline{T}$ dimensionless temperature [T/T_0]
T_{atm} : temperature of the atmosphere [K]
T, T_w : pellet or bed temperature and wall temperature, respectively [K]
t : time [s]
τ : dimensionless time [t^*u_0/L]
u : interstitial velocity [cm/s]
$\overline{u}$: dimensionless velocity [u/u_0]
y_i : mole fraction of species i in the gas phase
z : axial distance in the bed from the inlet [cm]
$\overline{z}$: dimensionless length

Greek Letters

α : particle porosity
β : equilibrium parameter for the Langmuir model in the form of dimensionless
ε, ε_t : voidage of the adsorbent bed and total void fraction, respectively
ρ_g, ρ_p, ρ_B, ρ_w : gas density, pellet density, bulk density, and bed wall density, respectively [g/cm^3]

Subscripts

B : bed
H : higher operating pressure
i : component i
L : lower operating pressure
p : pellet
g : gas phase
s : solid
w : wall

REFERENCES

1. C. A. Grande, Advances in Pressure Swing Adsorption for Gas Separation, ISRN Chemical Engineering, Article ID 982934, **2012**, 13 (2012), DOI:10.5402/2012/982934.
2. M. Rosen, L. Mulloth, D. Affleck and Y. Wang, Development and Testing of a Temperature-Swing Adsorption Compressor for Carbon Dioxide in Closed-Loop Air Revitalization Systems, SAE Technical Paper 2005-01-2941 (2005), DOI:10.4271/2005-01-2941.
3. R. M. Milton, Molecular Sieve Adsorbents, US Patent, 2,882,243 (1959).
4. A. Mivechian and M. Pakizeh, *Korean J. Chem. Eng.*, **30**(4), 937 (2013).
5. S.-C. Jang, S.-I. Yang, S.-G. Oh and D.-K. Choi, *Korean J. Chem. Eng.*, **28**(2), 583 (2011).
6. Y. H. Kim, D. G. Lee, D. K. Moon, S.-H. Byeon, H. Ahn and C. H. Lee, *Korean J. Chem. Eng.*, **31**(1), 132 (2014), Available from: 10.1007/s11814-013-0201-x.
7. M. Zaman and J. H. Lee, *Korean J. Chem. Eng.*, **30**(8), 1497 (2013).
8. V. Hoshyargar, F. Fadaei and S. N. Ashrafizadeh, *Korean J. Chem. Eng.*, **32**(7), 1388 (2015).
9. D. M. Ruthven, S. Farooq and K. S. Knaebel, *Pressure Swing Adsorption*, New York, VCH Publications, Inc. (1994).
10. R. T. Yang, *Adsorbents: Fundamentals and Applications*, New Jersey, Wiley (2003).
11. D. M. Ruthven, *Principle of Adsorption and Adsorption Processes*, New York, Wiley (1984).
12. C. Chou and W.-C. Huang, *Ind. Eng. Chem. Res.*, **33**(5), 1250 (1994).
13. L. Lin, *Numerical Simulation of Pressure Swing Adsorption Process*, Dissertation Presented for the Degree of Bachelor of Science, XIDIAN University, Xi'an, China (1990).
14. J. A. Ritter and Y. Liu, *Ind. Eng. Chem. Res.*, **37**, 2783 (1998).
15. K. G. Teague, Jr. and T. F. Edgar, *Ind. Eng. Chem. Res.*, **38**, 3761 (1999).
16. A. M. M. Mendes, C. A. V. Costa and A. E. Rodrigues, *Ind. Eng. Chem. Res.*, **39**, 138 (2000).
17. A. M. M. Mendes, C. A. V. Costa and A. E. Rodrigues, *Sep. Purif. Technol.*, **24**, 173 (2001).
18. S. J. Wilson, C. C. K. Beh, P. A. Webley and R. S. Todd, *Ind. Eng. Chem. Res.*, **40**, 2702 (2001).
19. S. U. Rege, R. T. Yang, K. Qian and M. A. Buzanowski, *Chem. Eng. Sci.*, **56**, 2745 (2001).
20. J. G. Jee, J. S. Lee and C. H. Lee, *Ind. Eng. Chem. Res.*, **40**, 3647 (2001).
21. J. G. Jee, S. J. Lee and C. H. Lee, *Korean J. Chem. Eng.*, **21**, 1183 (2004).
22. J. G. Jee, H. G. Park, S. J. Haam and C. H. Lee, *Ind. Eng. Chem. Res.*, **41**, 4383 (2002).

23. S. T. Y. Choong, W. R. Paterson and D. M. Scott, *Jurnal Teknologi*, **38**, 65 (2003).
24. J. C. Santos, A. F. Portugal, F. D. Magalhaes and A. Mendes, *Ind. Eng. Chem. Res.*, **43**, 8328 (2004).
25. S. P. Reynolds, A. D. Ebner and J. A. Ritter, *Ind. Eng. Chem. Res.*, **45**, 3256 (2006).
26. K. P. Kostroski and P. C. Wankat, *Ind. Eng. Chem. Res.*, **45**, 8117 (2006).
27. J.-G. Jee, M.-K. Park, H.-K. Yoo, K. Lee and C.-H. Lee, *Sep. Sci. Technol.*, **37**(5), 3465 (2002).
28. S. J. Lee, J. H. Jung, J. H. Moon, J. G. Jee and C. H. Lee, *Ind. Eng. Chem. Res.*, **46**, 3720 (2007).
29. M. Mofarahi and J. S. Ehsan, *Petroleum Coal*, **55**(3), 216 (2013).
30. T. N. Olney, N. M. Cann, G. Cooper and C. E. Brion, *Chem. Phys.*, **223**(1), 59 (1997).
31. S. Jain, A. S. Moharir, P. Li and G. Wozny, *Sep. Purif. Technol.*, **33**, 25 (2003).